5G Positioning and Mapping with Diffuse Multipath

N.B. When citing this work, cite the original published paper.

(article starts on next page)

5G Positioning and Mapping with Diffuse Multipath

Fuxi Wen, *Senior Member, IEEE*, Josef Kulmer, *Student Member, IEEE*, Klaus Witrisal, *Member, IEEE* and Henk Wymeersch, *Senior Member, IEEE*

Abstract—5G mmWave communication is useful for positioning due to the geometric connection between the propagation channel and the propagation environment. Channel estimation methods can exploit the resulting sparsity to estimate parameters (delay and angles) of each propagation path, which in turn can be exploited for positioning and mapping. When paths exhibit significant spread in either angle or delay, these methods break down or lead to significant biases. We present a novel tensor-based method for channel estimation that allows estimation of mmWave channel parameters in a non-parametric form. The method is able to accurately estimate the channel, even in the absence of a specular component. This in turn enables positioning and mapping using only diffuse multipath. Simulation results are provided to demonstrate the efficacy of the proposed approach.

Index Terms—massive MIMO, localization, beamspace ES-PRIT, tensor decomposition, subspace.

I. INTRODUCTION

5G mmWave signals present unique opportunities for positioning or user devices, due to their large bandwidths, arrays with many antenna elements and favorable propagation conditions [1]. 5G mmWave is currently a study item for 3GPP-R17 and has the potential not only to provide performance better than Global Positioning System (GPS), but also enable precise orientation estimation. Moreover, due to the high degree of resolvability of propagation paths, multipath information can naturally be exploited, both for positioning as well as for mapping of the environment [2] Applications of 5G mmWave positioning include traditional emergency call localization and personal navigation, but also more disruptive topics such as localization or robots and autonomous vehicles, as well as augmented and virtual reality applications.

In order to develop a localization method, an understanding of the mmWave channel is needed. mmWave propagation, occurring at carrier frequencies above 24 GHz, has been shown to be characterized by limited scattering, no diffraction and shadowing, and the existence of only a few propagation paths. Each of the paths is thus largely determined by the propagation environment and characterized by channel gains, angles of arrival, angles of departure, and delays. Propagation paths may be of a deterministic specular nature, when the surface on which waveforms impinge is sufficiently smooth, or of a stochastic diffuse/scattering nature when the surface is relatively rough, or a combination of both. Hence, in general, each path (except the line-of-sight (LOS) path) is in fact a cluster of paths, with similar angles and delays [3]. When the paths within a cluster are not resolvable in either angles or delays, they lead to fluctuations in the received power. This is the model typically assumed in the communication literature. On the other hand, when intra-cluster paths are resolvable, they should be properly estimated in order to avoid biasing the estimation of angles and delays.

A cluster can be characterized in multiple ways. Traditionally, a statistical model has been considered, whereby a cluster is modeled though a mean and a spread in both angle and delay domain [4]. Given such a model, there is a rich literature on second-order estimation methods that are able to accurately and blindly estimate the mean and spread of a cluster [5], [6]. The models for spatially distributed sources have been classified into two types, namely incoherently distributed (ID) sources and coherently distributed (CD) sources. On one hand, for ID sources, signals coming from different points of the same distributed source can be considered as uncorrelated [7]–[10]. On the other hand, in the scenario of CD sources, the received signal components are delayed and scaled replicas from different points within the same source [11]–[13]. In [14], the performance bound is studied of the tracking accuracy in sparse mmWave channels that includes cluster angular spreads. However, while such subspace methods are powerful, in the context of mmWave communication, the signal structure and presence of dedicated pilot signals should be exploited to develop faster methods. There is thus a lack of first-order methods for quickly estimating channel parameters and their spread. This explains why 5G mmWave localization has considered either only the LOS path, or treated multipath as purely specular [15]–[17]. Standard 5G mmWave channel estimation is based on either compressive sensing approaches [18], which express the sparsity in an appropriate domain, or on tensor decompositions, where the dominant higher-order singular values can be related to the dominant signal paths [19], [20]. A joint tensor decomposition and compressed sensing based multidimensional channel parameter estimation method is proposed in [21]. However, these methods do not account for the intra-cluster spread of angles or delay. Both matrix-based and tensor-based approaches can be applied for channel estimation in localization. In the traditional channel estimation approaches, the multi-dimensional signals are stored in matrices by means of a stacking operation. Obviously, this representation does not account for the R-D grid structure inherent in the data. Hence, a more natural approach to store and manipulate the R-D data is given by tensors, leading to better performance than matrix-based methods.

In this paper, we propose a tensor-based method for estimating a 5G mmWave channel in terms of the angles and delays of the individual paths within each non-line-of-sight (NLOS)

cluster. The method makes no a priori assumption regarding the number of paths per cluster. The problem of clustering is not our focus, and standard clustering methods can be applied, such as k-means and density-based spatial clustering of applications with noise (DBSCAN) [22]. Following a clustering of paths, the statistics of each cluster can be determined, which are finally fed to a search-free positioning and mapping method, which operates with lower complexity than optimization [15] or message passing methods [16], [17], designed only for specular multipath. The proposed method is able to determine the dominant clusters and accurately estimate the cluster statistics, even for clusters that have no specular component. Building on this, we present a positioning and mapping method that accurately localizes the user and maps the environment by exploiting the diffuse multipath, rather than considering it as a disturbance. As an extension, [23] provides insights into cases not covered by this paper, namely synchronization and orientation estimation are important in practice. Our main contributions are the following:

- We derive a novel method for estimating mmWave channels in the presence of combined specular and scattered components, based on a tensor decomposition.
- We provide a detailed evaluation of the proposed method in a three-dimensional propagation environment, demonstrating its performance under varying levels of surface roughness.
- We propose a low complexity, search-free 5G mmWave localization and mapping method that is able to operate in the absence of LOS and specular multipath. The method can operate using only the diffuse multipath for positioning and mapping.

II. TENSORS AND TENSOR OPERATIONS

A. Definitions and Notations

The tensor operations used in this paper are consistent with [24]. An R-D tensor is denoted by $\boldsymbol{\mathcal{A}} \in \mathbb{C}^{M_1 \times M_2 \times \cdots \times M_R}$, where M_r is the size of the rth mode of the tensor and $R \geq 3$. We use $a_{m_1, m_2, \cdots, m_R}$ to represent the $(m_1, m_2, \cdots, m_R)$ entry.

Unfolding: The r-mode unfolding of $\boldsymbol{\mathcal{A}}$ is written as $\mathbf{A}_{(r)} \in \mathbb{C}^{M_r \times (M_1 \cdots M_{r-1} M_{r+1} \cdots M_R)}$ where the order of the columns is chosen according to Definition 1 in [25].

Product: The r-mode product of a tensor $\boldsymbol{\mathcal{A}} \in \mathbb{C}^{M_1 \times M_2 \times \cdots \times M_R}$ and a matrix $\mathbf{U} \in \mathbb{C}^{N_r \times M_r}$ along the rth mode is denoted as Definition 8 in [25],

$$\boldsymbol{\mathcal{B}} = \boldsymbol{\mathcal{A}} \times_r \mathbf{U} \in \mathbb{C}^{M_1 \times \cdots \times M_{r-1} \times N_r \times M_{r+1} \times \cdots \times M_R}. \quad (1)$$

Concatenation: We use the operator $[\boldsymbol{\mathcal{A}}_1 \sqcup_{R+1} \boldsymbol{\mathcal{A}}_2] \in \mathbb{C}^{M_1 \times M_2 \times \cdots \times M_R \times 2}$ to represent the concatenation of two tensors $\boldsymbol{\mathcal{A}}_1 \in \mathbb{C}^{M_1 \times M_2 \times \cdots \times M_R}$ and $\boldsymbol{\mathcal{A}}_2 \in \mathbb{C}^{M_1 \times M_2 \times \cdots \times M_R}$, along the $(R+1)$th mode [26].

B. Tensor Decompositions

There exist various decompositions of tensors and definitions of the rank of a tensor. We consider here the CAN-DECOMP/PARAFAC (CP) decomposition and the Tucker decomposition.

CP decomposition decomposes an R-D tensor $\boldsymbol{\mathcal{X}}$ as a sum of rank-one tensors

$$\boldsymbol{\mathcal{X}} = \sum_{d=1}^{D} \gamma_d \mathbf{a}_d^{(1)} \circ \mathbf{a}_d^{(2)} \ldots \circ \mathbf{a}_d^{(R)}, \quad (2)$$

where $\circ$ denotes outer product. The rank D of a tensor is defined as the smallest number of rank one tensors that generate $\boldsymbol{\mathcal{X}}$ as their sum. In other words, it is the smallest number of components in an exact CP decomposition [27], [28]. The r-rank of a tensor is the column rank of $\boldsymbol{\mathcal{X}}_{(r)}$ [29]. *Tucker decomposition* is a form of higher-order principal component analysis. It decomposes a tensor into a core tensor multiplied (or transformed) by a matrix along each mode. The matrix can be thought of as the principal components in each mode.

III. SYSTEM MODEL

We consider a 3-dimensional ($3D$) scenario with a single 5G transmitter with known location $\boldsymbol{p}_T$ and orientation, a receiver with unknown location $\boldsymbol{p}_R$, and a physical propagation environment, characterized by surfaces, as depicted in Figure 1. The transmitter and receiver both employ uniform rectangular arrays (URAs) consist of sensors in a grid of size $M_T = M_1 \times M_2$ and $M_R = M_3 \times M_4$, and exchange MIMO-OFDM signals with M_5 sub-carriers and sub-carrier spacing Δ_f. The received signal on subcarrier i is of the form

$$\mathbf{Y}_i = \mathbf{H}_i \mathbf{S}_i + \mathbf{N}_i \in \mathbb{C}^{M_R \times T}, \quad (3)$$

where $\mathbf{S}_i \in \mathbb{C}^{M_T \times T}$ is a known pilot signal spanning $T \geq M_T$ OFDM symbols with orthogonality property ($\mathbf{S}_i \mathbf{S}_i^{\mathsf{H}}$ is a scaled identity matrix) and $\mathbf{N}_i$ is i.i.d. Gaussian noise. Then we have

$$\mathbf{Y}_i \mathbf{S}_i^{\mathsf{H}} = \mathbf{H}_i + \mathbf{N}_i \mathbf{S}_i^{\mathsf{H}}. \quad (4)$$

For subcarrier i, we receive $\mathbf{Y}_i \mathbf{S}_i^{\mathsf{H}}$, which is an $M_3 M_4 \times M_1 M_2$ matrix. Then we convert these M_5 matrices $\mathbf{Y}_i \mathbf{S}_i^{\mathsf{H}}, i = 1, 2, \cdots, M_5$ (one per subcarrier) in a 5D tensor of suitable dimension, $\boldsymbol{\mathcal{Y}} \in \mathbb{C}^{M_1 \times M_2 \times M_3 \times M_4 \times M_5}$. The channel matrix $\mathbf{H}_i$ depends on the array structure and the propagation environment, described next. Our aim is to determine $\boldsymbol{p}_R$ and map the propagation environment.

A. Array Steering Vector for URA

The transmit and receive arrays are planar arrays, comprising omni-directional elements on a uniform grid of rectangular shape with inter-element spacing equal to half of the signal's wavelength. Transmit and receive URAs consist of sensors are indexed by (m_1, m_2) and (m_3, m_4), respectively.

The URA steering vector corresponding to the lth source can be formed as

$$\mathbf{a}(\omega_{l,1}, \omega_{l,2}) = \mathbf{a}(\omega_{l,1}) \otimes \mathbf{a}(\omega_{l,2}), \quad (5)$$

where $\otimes$ is Kronecker product, $\mathbf{a}(\omega_{l,1}) = [a_1(\omega_{l,1}) \cdots a_{m_1}(\omega_{l,1}) \cdots a_{M_1}(\omega_{l,1})]^{\mathsf{T}}$ and $\mathbf{a}(\omega_{l,2}) = [a_1(\omega_{l,2}) \cdots a_{m_2}(\omega_{l,2}) \cdots a_{M_2}(\omega_{l,2})]^{\mathsf{T}}$ are equivalent to the uniform linear array steering vectors composed of M_1 and
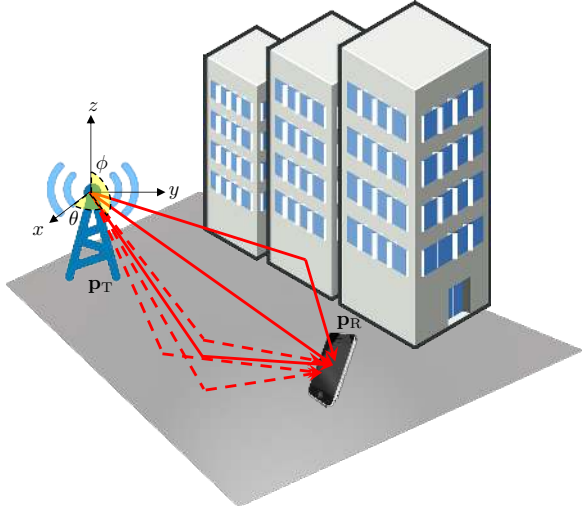
Fig. 1. Illustration of the considered scenario with 1 LOS path and 2 NLOS clusters (i.e., $K = 3$).

M_2 sensors lying on y-axis and z-axis, respectively. The first sensor is taken as the reference sensor so that (up to a global phase)

$$a_m(\omega) = e^{j(m-1)\omega}. \tag{6}$$

The spatial frequencies associated with the azimuth θ_l and elevation angle ϕ_l of the lth source follow as

$$\omega_{l,1} = \pi \sin(\theta_l) \sin(\phi_l), \quad \omega_{l,2} = \pi \cos(\phi_l). \tag{7}$$

B. Channel Model

We propose a generative model for simulating the diffuse multipath of mmWave channels, based on [30], [31]. This model starts from generating points on the surface, based on the its roughness. Then, for each point, the channel parameters are computed (angles, delay, gains). Finally, the model is expressed in a tensor representation. For smooth reflective surfaces, the model reverts to the one used in [15].

1) Surface Roughness and Scattering: The propagation environment consists of K well-separated clusters, each cluster k corresponds to a physical object (e.g., a wall, a ground reflection), described by MPCs, characterized by two parameters [30], [31]:

- The scattering coefficient $S \in [0, 1]$, which quantifies the relative amount (with respect to absorption) of total scattered amplitude, and was identified to be $S \geq 0.4$ [31], [32].
- The directivity parameter $\alpha_R \geq 0$ which describes the width of the scattering lobe originating at the reflective surface. At rough surfaces (in comparison to the signal's wavelength), the scattering power has a large intra-cluster spread, corresponding to a small directivity $\alpha_R \rightarrow 0$. At smooth surfaces, the spread of scattering power is reduced, equivalent to more directivity $\alpha_R \rightarrow \infty$. Hence, α_R may be associated to surface roughness. Typical values are in a range of $\alpha_R \in \{1, \ldots, 11\}$ [31], [32].

Combined, α_R and S can be used to determine the cluster power and cluster spread through the joint angular delay

power spectrum (JADPS) which describes the scattered power $p_{\text{DM}}(\boldsymbol{p})$ from any point $\boldsymbol{p}$ [30]. Cluster k gives rise to L_k scatter points, where the total number of paths is $P = \sum_{k=1}^{K} L_k$. For the LOS path, $L_k = 1$. Each scatter point $\boldsymbol{p}_{kl} \in \mathbb{R}^3$ lies on the k-th surface with scatter point index $0 < l \leq L_k$.

2) Generation of Channel Parameters: Given a path between $\boldsymbol{p}_{\text{R}}$ and $\boldsymbol{p}_{\text{T}}$ via $\boldsymbol{p}_{kl}$, the path delay τ_{kl}, as well as azimuth and elevation angles of the angle-of-departure (AOD) (θ_{kl}, ϕ_{kl}) and of the angle-of-arrival (AOA) $(\vartheta_{kl}, \varphi_{kl})$ follow from standard geometry and can be found in the Appendix A. Finally, each path from a scatter point has a gain γ_{kl}, which we propose to comprise a constant amplitude per cluster and a random phase, uniform over $[0, 2\pi)$. Motivation and additional details of this model are provided in Appendix B.

3) Tensor Formulation: Let

$$\omega_{kl,1} = \pi \sin(\theta_{kl}) \sin(\phi_{kl}), \quad \omega_{kl,2} = \pi \cos(\phi_{kl}), \tag{8}$$

and

$$\omega_{kl,3} = \pi \sin(\vartheta_{kl}) \sin(\varphi_{kl}), \quad \omega_{kl,4} = \pi \cos(\varphi_{kl}), \tag{9}$$

the channel response in frequency domain for sub-carrier i with frequency f_i is represented as [33]

$$\mathbf{H}_i = \sum_{k=1}^{K} \sum_{l=1}^{L_k} \gamma_{kl} e^{-j2\pi f_i \tau_{kl}} \mathbf{a}_{\text{R}}(\vartheta_{kl}, \varphi_{kl}) \mathbf{a}_{\text{T}}^{\mathsf{H}}(\theta_{kl}, \phi_{kl}), \tag{10}$$

where

$$\mathbf{a}_{\text{T}}(\omega_{kl,1}, \omega_{kl,2}) = \mathbf{a}(\omega_{kl,1}) \otimes \mathbf{a}(\omega_{kl,2}) \in \mathbb{C}^{M_T \times 1}, \tag{11}$$

and

$$\mathbf{a}_{\text{R}}(\omega_{kl,3}, \omega_{kl,4}) = \mathbf{a}(\omega_{kl,3}) \otimes \mathbf{a}(\omega_{kl,4}) \in \mathbb{C}^{M_R \times 1}. \tag{12}$$

For subcarrier i, $\mathbf{H}_i$ is an $M_3 M_4 \times M_1 M_2$ matrix. Then we convert these M_5 matrices (one per subcarrier) in a 5D tensor of suitable dimension, $\boldsymbol{\mathcal{H}} \in \mathbb{C}^{M_1 \times M_2 \times M_3 \times M_4 \times M_5}$.

IV. PROPOSED METHOD

We now present our method for localizing the receiver and the cluster locations.

A. Tensor Representation

The $(m_1, m_2, m_3, m_4, m_5)$ entry of the channel response in frequency domain $\boldsymbol{\mathcal{H}} \in \mathbb{C}^{M_1 \times M_2 \times M_3 \times M_4 \times M_5}$ is described as

$$h_{m_1 m_2 m_3 m_4 m_5} = \sum_{k=1}^{K} \sum_{l=1}^{L_k} \gamma_{kl} a_{m_1}(\omega_{kl,1}) a_{m_2}(\omega_{kl,2})$$
$$a_{m_3}(\omega_{kl,3}) a_{m_4}(\omega_{kl,4}) a_{m_5}(\omega_{kl,5}), \tag{13}$$

where the spatial frequency $\omega_{kl,5} = 2\pi \Delta_f \tau_{kl}$, and $a_m(\omega)$ is defined in (6). The response can be described as a CP model (sum of P rank-one tensors),

$$\boldsymbol{\mathcal{H}} = \sum_{p=1}^{P} \gamma_p \mathbf{a}_{p,1} \circ \mathbf{a}_{p,2} \circ \mathbf{a}_{p,3} \circ \mathbf{a}_{p,4} \circ \mathbf{a}_{p,5}. \tag{14}$$

For $r = 1, 2, \cdots, 5$,

$$\mathbf{a}_{p,r} = \begin{bmatrix} a_1(\omega_{p,r}) & a_2(\omega_{p,r}) & \cdots & a_{M_r}(\omega_{p,r}) \end{bmatrix}^{\mathsf{T}}. \tag{15}$$

The array manifold for the rth dimension is defined as

$$\mathbf{A}_r = \begin{bmatrix} \mathbf{a}_{1,r} & \cdots & \mathbf{a}_{p,r} & \cdots & \mathbf{a}_{P,r} \end{bmatrix} \in \mathbb{C}^{M_r \times P}. \quad (16)$$

For multiple measurement scenarios, the augmented observation tensor is described as

$$\boldsymbol{\mathcal{Y}} = \big[\underbrace{\boldsymbol{\mathcal{H}} \sqcup_6 \cdots \boldsymbol{\mathcal{H}}}_{M_6}\big] + \boldsymbol{\mathcal{N}} \in \mathbb{C}^{M_1 \times M_2 \times M_3 \times M_4 \times M_5 \times M_6}, \quad (17)$$

where M_6 is the subsequent time instants, $\boldsymbol{\mathcal{N}}$ is the noise tensor.

B. Multipath Components (MPC) Parameter Estimation

1) Estimate the number of paths P: To estimate geometrical parameters such as AOD, AOA and delay, the first step is to estimate the number $\hat{P}$ of signal components in (14). In the CP model, a tensor is decomposed into a sum of rank-one tensors, which are expressed as the outer product of vectors. In practice, each rank-one component corresponds to a natural source or signal. Finding the tensor rank or number of multilinear components in the underlying CP model of noisy tensor observations is an important research topic. Existing approaches to CP rank estimation from noisy observations include [28].

R-D minimum description length (MDL) [29] is utilized for tensor rank estimation, which is proposed by stacking the measurement tensor into a matrix with the r-mode unfolding operation,

$$\boldsymbol{\mathcal{Y}} \xrightarrow[\text{unfolding}]{r\text{-mode}} \mathbf{Y}_{(r)}. \quad (18)$$

The eigenvalue spectrum $\boldsymbol{\Lambda}_r$ obtained from the singular value decomposition (SVD) of $\mathbf{Y}_{(r)}$ and MDL are used for r-rank $\hat{P}_r$ estimation,

$$\mathbf{Y}_{(r)} \xrightarrow{\text{SVD}} \boldsymbol{\Lambda}_r \xrightarrow{\text{MDL}} \hat{P}_r. \quad (19)$$

After obtaining r-rank, the tensor rank is estimated as

$$\hat{P} = \max\{\hat{P}_1, \hat{P}_2, \cdots, \hat{P}_R\}, \quad (20)$$

to ensure a high number of estimated paths, required for cluster mean and cluster spread estimation. In general, $\hat{P}_r \ll P$, so the rank is always underestimated.

2) Angle and Delay Estimation: After estimating the number of resolvable signal components $\hat{P}$, an R-D subspace is obtained via CP Decomposition [34]. For URA, tensor or N-D ESPRIT [24], [35], [36] is applied for channel parameter estimation. The standard conditions for tensor ESPRIT hold for the specular components, but not for the diffuse ones. Hence, it is not possible to recover the dense physical scattering points (SPs) related to diffuse multipath. Instead we recover angles and delays from artificial resolved SPs. If the physical environment comprised the specular paths and the artificial SPs, again the conditions for tensor ESPRIT would hold. Let $\mathbf{U}_r \in \mathbb{C}^{M_r \times \hat{P}}$ be the subspace spanned by $\mathbf{A}_r \in \mathbb{C}^{M_r \times \hat{P}}$, which is obtained by applying CP decomposition on $\boldsymbol{\mathcal{Y}}$. The main idea of tensor-ESPRIT is exploiting the multidimensional shift invariance property of the measurements. For each dimension, the array is divided into two subarrays with same number of elements. The subarrays may overlap and an element may

be shared by the two subarrays. For the rth dimension, we have

$$\mathbf{A}_r = \mathbf{U}_r \mathbf{D}_r, \quad (21)$$

where $\mathbf{D}_r \in \mathbb{C}^{\hat{P} \times \hat{P}}$ is a non-singular matrix. We further define two sub-matrices,

$$\mathbf{U}_{1,r} = \mathbf{J}_{1,r}^{(n)} \mathbf{U}_r \text{ and } \mathbf{U}_{2,r} = \mathbf{J}_{2,r}^{(n)} \mathbf{U}_r, \quad (22)$$

where $\mathbf{J}_{1,r}$ and $\mathbf{J}_{2,r}$ are two selection matrices,

$$\begin{aligned} \mathbf{J}_{1,r}^{(n)} &= \begin{bmatrix} \mathbf{I}_{M_r-n} & \mathbf{0}_{(M_r-n)\times n} \end{bmatrix}, \\ \mathbf{J}_{2,r}^{(n)} &= \begin{bmatrix} \mathbf{0}_{(M_r-n)\times n} & \mathbf{I}_{M_r-n} \end{bmatrix}, \end{aligned} \quad (23)$$

where $\mathbf{I}_n$ denotes identity matrix of size $n \times n$ and $\mathbf{0}_{m \times n}$ denotes zero matrix of size $m \times n$. For convenience, we focus on $n = 1$, $\mathbf{J}_{1,r}^{(n)}$ and $\mathbf{J}_{2,r}^{(n)}$ are simplified as $\mathbf{J}_{1,r}$ and $\mathbf{J}_{2,r}$. Then we have

$$\mathbf{J}_{1,r} \mathbf{A}_r = \mathbf{J}_{2,r} \mathbf{A}_r \boldsymbol{\Phi}_r, \quad (24)$$

where

$$\boldsymbol{\Phi}_r = \text{diag} \begin{bmatrix} e^{-j\omega_{1,r}} & e^{-j\omega_{2,r}} & \cdots & e^{-j\omega_{\hat{P},r}} \end{bmatrix}. \quad (25)$$

Substituting (21) and (22) into (24), we have

$$\mathbf{U}_{1,r} = \mathbf{U}_{2,r} \boldsymbol{\Psi}_r, \quad (26)$$

where

$$\boldsymbol{\Psi}_r = \mathbf{D}_r \boldsymbol{\Phi}_r \mathbf{D}_r^{-1} \in \mathbb{C}^{\hat{P} \times \hat{P}}. \quad (27)$$

The equations in (24) are over-determined. The simplest choice to estimate $\boldsymbol{\Psi}_r$ is using the least squares (LS) method and the resulting closed-form solution is given by

$$\hat{\boldsymbol{\Psi}}_r = (\mathbf{U}_{2,r})^\dagger \mathbf{U}_{1,r}, \quad (28)$$

where $\dagger$ denotes the Moore-Penrose matrix inverse. Let $\lambda_{1,r}, \lambda_{2,r}, \cdots, \lambda_{\hat{P},r}$ be the eigenvalues of $\hat{\boldsymbol{\Psi}}_r$, the mode r frequencies are estimated by using

$$\omega_{p,r} = -\angle(\lambda_{p,r}), p = 1, 2, \cdots, \hat{P}, \quad (29)$$

where $\angle(\cdot)$ denotes the argument of a complex number.

Remark 1. *The method can be generalized to beam-space tensor ESPRIT for hybrid URA structure [37] and beam-space tensor MUSIC for a hybrid arbitrary array geometry [13].*

3) Clustering the MPCs: Clustering techniques, such as k-means are applied to group the 5-D parameters of the estimated $\hat{P}$ multi-path components $\boldsymbol{\omega}_p = \begin{bmatrix} \omega_{p,1} & \omega_{p,2} & \cdots & \omega_{p,5} \end{bmatrix}$. It can be extended to other techniques such as connectivity-based, distribution-based and density-based [38]. Given a set of estimates $\{\boldsymbol{\omega}_p, p = 1, 2, \cdots, \hat{P}\}$, our objective is to partition the data set into K clusters, we assume that the value of K is given or can be estimated from model order selection techniques [39]. Recently, the challenges and opportunities in clustering-enabled wireless channel modeling were discussed in [40]. A framework of automatic clustering and tracking algorithm was proposed for the MPCs in time-variant radio channels [41].

The clustering problem can be formalized by introducing a set of vectors $\{\boldsymbol{\mu}_k, k = 1, 2, \cdots, K\}$, in which $\boldsymbol{\mu}_k \in \mathbb{R}^{D \times 1}$ represents the center of the kth cluster. The motivation is to
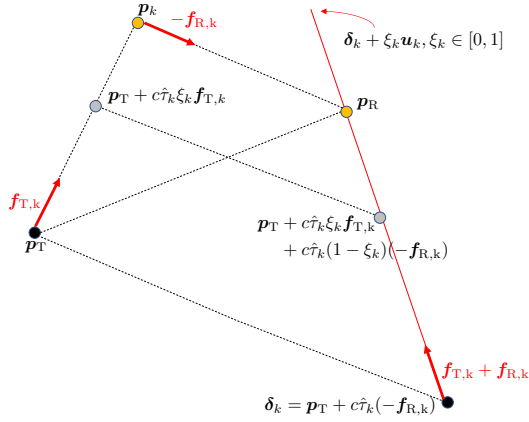
Fig. 2. The proposed method for localization and mapping. The locations $\boldsymbol{p}_{\mathrm{R}}$ and $\boldsymbol{p}_k$ (one for each of the $\hat{P}$ estimated paths) are unknown (in orange). The vectors $\boldsymbol{f}_{\mathrm{T},k}$ and $\boldsymbol{f}_{\mathrm{R},k}$, as well as the total path length are known, based on the measurements. The locations in grey are possible hypotheses of where $\boldsymbol{p}_{\mathrm{R}}$ and $\boldsymbol{p}_k$ may be, parameterized by $\xi_k \in [0,1]$. Each value of ξ_k leads to a point on the line shown in red. The receiver must this lie on the intersection of these lines.

assign the data set to clusters, such that the distances of each data to its closest cluster center is minimized. The objective can be rewritten in terms of the total distortion

$$\mathcal{J} = \sum_{p=1}^{\hat{P}} \sum_{k=1}^{K} z_{pk} \left\| \boldsymbol{\omega}_p - \boldsymbol{\mu}_k \right\|^2, \tag{30}$$

where $z_{pk} = 1$, if data point $\boldsymbol{\omega}_p$ is assigned to cluster k, otherwise $z_{pk} = 0$. Each example $\boldsymbol{\omega}_p$ is assigned or reassigned to its closest cluster center $\mathcal{C}_k$, if

$$\mathcal{C}_k = \{ n : k = \arg\min_k \left\| \boldsymbol{\omega}_p - \boldsymbol{\mu}_k \right\|^2 \}. \tag{31}$$

The cluster means are updated as

$$\boldsymbol{\mu}_k = \frac{1}{|\mathcal{C}_k|} \sum_{p \in \mathcal{C}_k} \boldsymbol{\omega}_p, \tag{32}$$

where $|\cdot|$ is the cardinality of a set, which measures the number of elements of the set. The cluster spread is defined as the standard deviation of all the $\boldsymbol{\omega}_p$ within the same cluster. Recall that all paths within a cluster have the same amplitude, so the mean and spread do not require weighting. Finally, MPC parameter estimates of AOD ($\hat{\theta}_k, \hat{\phi}_k$), AOA ($\hat{\vartheta}_k, \hat{\varphi}_k$) and delay $\hat{\tau}_k$ are calculated from spatial frequencies in $\boldsymbol{\mu}_k$ as stated in Sec. III-B3.

C. Mapping and Localization

The localization and mapping problem can be expressed as a maximum likelihood problem:

$$[\hat{\boldsymbol{p}}_{\mathrm{R}}, [\hat{\boldsymbol{p}}_k]_{k=1}^{\hat{P}}] \tag{33}$$
$$= \arg\max_{\boldsymbol{p}_{\mathrm{R}}, [\boldsymbol{p}_k]_{k=1}^{\hat{P}}} p([\boldsymbol{\omega}_k]_{k=1}^{\hat{P}} | \boldsymbol{p}_{\mathrm{R}}, [\boldsymbol{p}_k]_{k=1}^{\hat{P}}, \boldsymbol{p}_{\mathrm{T}})$$
$$= \arg\max_{\boldsymbol{p}_{\mathrm{R}}, [\boldsymbol{p}_k]_{k=1}^{\hat{P}}} p([\hat{\tau}_k, \hat{\theta}_k, \hat{\phi}_k, \hat{\vartheta}_k, \hat{\varphi}_k]_{k=1}^{\hat{P}} | \boldsymbol{p}_{\mathrm{R}}, [\boldsymbol{p}_k]_{k=1}^{\hat{P}}, \boldsymbol{p}_{\mathrm{T}}).$$

To avoid a high-dimensional optimization and inference of hidden parameters (α_R and S), we propose a general search-free method based on [42] that does not rely on knowledge on whether or not the LOS path is present. We define

$$\boldsymbol{f}_{\mathrm{T},k} = \begin{bmatrix} \cos(\hat{\theta}_k)\sin(\hat{\phi}_k) \\ \sin(\hat{\theta}_k)\sin(\hat{\phi}_k) \\ \cos(\hat{\phi}_k) \end{bmatrix}, \tag{34}$$

which points along the direction of departure of path $k \in \{1, \ldots, \hat{P}\}$; and $\boldsymbol{f}_{\mathrm{R},k}$ is defined equivalently for the direction of arrival. For each cluster k we can establish a relation to $\boldsymbol{p}_{\mathrm{R}}$ according to

$$\boldsymbol{p}_{\mathrm{R}} = \boldsymbol{p}_{\mathrm{T}} + c\hat{\tau}_k \xi_k \boldsymbol{f}_{\mathrm{T},k} + c\hat{\tau}_k (1 - \xi_k)(-\boldsymbol{f}_{\mathrm{R},k}), \tag{35}$$

with unknown $\xi_k \in [0,1]$, representing the fraction of the path delay that is ascribed to the line from the BS to an artificial SP. Note that for the LOS path (if it is present), the value of ξ_k is arbitrary. In Fig. 2, we show the relation between the different defined vectors and the user location. Rearranging results in the line equation for each k as

$$\boldsymbol{p}_{\mathrm{R}} = \boldsymbol{\delta}_k + \xi_k \boldsymbol{u}_k, \tag{36}$$

with $\boldsymbol{\delta}_k = \boldsymbol{p}_{\mathrm{T}} - c\hat{\tau}_k \boldsymbol{f}_{\mathrm{R},k}$ and $\boldsymbol{u}_k = c\hat{\tau}_k(\boldsymbol{f}_{\mathrm{T},k} + \boldsymbol{f}_{\mathrm{R},k})$. The intersection of these lines determines the estimate of $\boldsymbol{p}_{\mathrm{R}}$. Specifically, we consider the cost function

$$C(\boldsymbol{p}_{\mathrm{R}}) = \sum_{k=1}^{\hat{P}} \zeta_k \left\| \boldsymbol{p}_{\mathrm{R}} - \left(\boldsymbol{\delta}_k + \bar{\boldsymbol{u}}_k^{\mathsf{T}}(\boldsymbol{p}_{\mathrm{R}} - \boldsymbol{\delta}_k)\bar{\boldsymbol{u}}_k \right) \right\|^2, \tag{37}$$

as sum of distance between $\boldsymbol{p}_{\mathrm{R}}$ and each path (36), $\zeta_k \geq 0$ is the weight of the k-th path (e.g., dependent on the SNR or the spread of path) and $\bar{\boldsymbol{u}}_k = \boldsymbol{u}_k / \|\boldsymbol{u}_k\|$. The least-squares solution becomes

$$\hat{\boldsymbol{p}}_{\mathrm{R}} = \left(\sum_{k=1}^{\hat{P}} \zeta_k (\boldsymbol{I} - \bar{\boldsymbol{u}}_k \bar{\boldsymbol{u}}_k^{\mathsf{T}}) \right)^{-1} \sum_{k=1}^{\hat{P}} \zeta_k (\boldsymbol{I} - \bar{\boldsymbol{u}}_k \bar{\boldsymbol{u}}_k^{\mathsf{T}}) \boldsymbol{\delta}_k. \tag{38}$$

Given $\hat{\boldsymbol{p}}_{\mathrm{R}}$, we can recover the scatter point $\boldsymbol{p}_k$ as intersection of the line equations $\boldsymbol{p}_{\mathrm{T}} + \zeta_{\mathrm{T}} \boldsymbol{f}_{\mathrm{T},k}, \zeta_{\mathrm{T}} \in \mathbb{R}$ and $\boldsymbol{p}_{\mathrm{R}} + \zeta_{\mathrm{R}} \boldsymbol{f}_{\mathrm{R},k}, \zeta_{\mathrm{R}} \in \mathbb{R}$ (see Fig. 2). The least-squares solution follows as

$$\hat{\boldsymbol{p}}_k = (\boldsymbol{H}_{\mathrm{T},k} + \boldsymbol{H}_{\mathrm{R},k})^{-1}(\boldsymbol{H}_{\mathrm{T},k}\boldsymbol{p}_{\mathrm{T}} + \boldsymbol{H}_{\mathrm{R},k}\hat{\boldsymbol{p}}_{\mathrm{R}}), \tag{39}$$

with $\boldsymbol{H}_{\mathrm{T},k} = \boldsymbol{I} - \boldsymbol{f}_{\mathrm{T},k}\boldsymbol{f}_{\mathrm{T},k}^{\mathsf{T}}$, $\boldsymbol{H}_{\mathrm{R},k} = \boldsymbol{I} - \boldsymbol{f}_{\mathrm{R},k}\boldsymbol{f}_{\mathrm{R},k}^{\mathsf{T}}$ and $\hat{\boldsymbol{p}}_{\mathrm{R}}$ from (38).

Note that the method does not require separation of specular and diffuse paths. The cost function in (37) can be applied with all $\hat{P}$ estimated paths, or only a selected subset of paths per cluster. In Section V-C, the performance of different options will be compared.

In the case multiple users are to be localized simultaneously, the proposed method can be applied independently by each individual user, based on the received downlink signals, as is currently done in LTE. Different levels of cooperation can be envisioned, including map sharing [43] and exploiting inter-user correlations [44].

Remark 2. *We note that the mapping and localization method does not require knowledge of the scattering coefficient S, the*

directivity α_R, or the locations of the physical scatter points. It is only required that the estimates $\boldsymbol{\omega}_p$ correspond to a 3D location.

D. Computational complexity

The most computationally demanding part of channel parameter estimation is the CP decomposition. In general, most CP decomposition algorithms, which factorize R-order tensors, face high computational cost due to computing gradients and (approximate) Hessians, line search and rotation. Table I in [45] summarizes the complexities of major computations in popular CP decomposition algorithms. For example, the alternating least squares (ALS) algorithm with line search has a complexity of order $\mathcal{O}\left(2^R PJ + RP^3\right)$, where $J = \prod_{r=1}^{R} M_r$ and P denotes the total number of paths. Having $\hat{P}$ multipaths, estimation of $\hat{\boldsymbol{p}}_R$ requires a single 3×3 matrix inversion, followed by $\hat{P} + 1$ matrix-vector multiplications. In addition, each scatter point estimate demands for a single 3×3 matrix inversion plus three matrix-vector multiplications. Finally, estimation of $\hat{\boldsymbol{p}}_R$ requires $\mathcal{O}(\hat{P})$ matrix-vector multiplications.

V. NUMERICAL RESULTS

A. Simulation Setup

We consider a carrier frequency of 28 GHz, corresponding to $\lambda = 1.07$ cm, a total bandwidth of 20 MHz with 100 subcarriers, of which 10 equally spaced subcarriers are used for pilots. A cyclic prefix of length 7 is used. 64 pilot OFDM symbols are sent, for a total duration of 3.52 ms. We set the pilots as $\mathbf{S}_i = \mathbf{I}, \forall i$. The surface reflection coefficient Γ is not specified, as we only use diffuse paths.

As shown in Fig. 3, the transmitter and receiver are located at $\boldsymbol{p}_T = [20, 0, 8]^\mathsf{T}$ and $\boldsymbol{p}_R = [0, 0, 2]^\mathsf{T}$, respectively, and are surrounded by two surfaces: one building facade and a ground surface. The building facade's center is at $[10, 10, 5]^\mathsf{T}$ with facade length of 20 m, facade height of 10 m, and orientation $[0, 1, 0]^\mathsf{T}$ (x-z plane). The ground surface is at $[10, 0, 0]^\mathsf{T}$ with orientation $[0, 0, 1]^\mathsf{T}$ (reflected from ground, x-y plane), surface dimension is 20×20 m. Both surfaces are described as rough surfaces *without specular component*, using $L_k = 100$ scatter points each. Furthermore, $K = 2$ is assumed for the following simulations and all the resolved paths are utilized for positioning and mapping, unless stated otherwise.

The transmitter is equipped with a uniform rectangular array (URA) with (8×8) elements and placed along y-z plane. In both directions, the inter-element spacing is 0.5λ. The origin is the array reference point. The receiver is also equipped with a URA with (8×8) elements and placed along y-z plane.

The Matlab package Tensorlab [46] is utilized for tensor computation, which provides several core algorithms for the computation of the CP decomposition including optimization-based methods such as alternating least squares (ALS), unconstrained nonlinear optimization and nonlinear least squares (NLS). By default, NLS is used for the CP decomposition. It can handle the partially distinct channel parameter scenarios, which was also validated in [47].
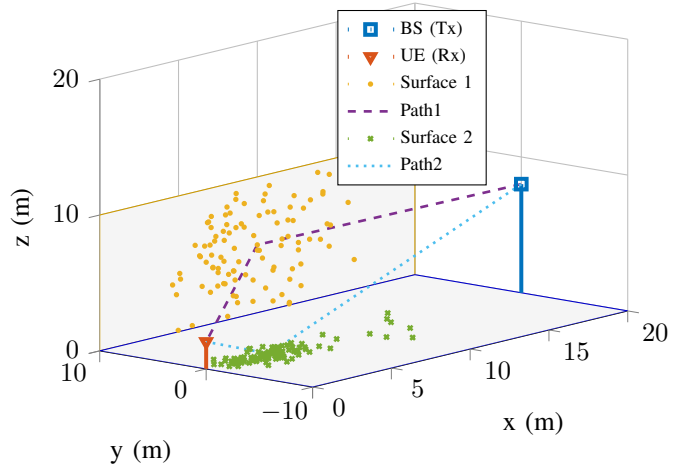

Fig. 3. Simulation setup for channel estimation and positioning performance evaluation with 2 clusters of different orientation and sizes.

TABLE I
RMSE OF CLUSTER MEAN (TOP) AND SPREAD (BOTTOM) - DENSE COMPONENTS, FOR VARIOUS LEVELS OF SNR

RMSE	SNR in dB		
$S = 0.8, \alpha_R = 10$	-10	0	10
Delay (meter)	0.3216	0.2025	0.1587
Azimuth AOD (degree)	2.8856	2.7250	2.1715
Elevation AOD (degree)	2.6749	2.2290	3.0189
Azimuth AOA (degree)	2.0951	1.4472	1.4027
Elevation AOA (degree)	2.4903	1.5805	1.2407

RMSE	SNR in dB		
$S = 0.8, \alpha_R = 10$	-10	0	10
Delay (meter)	0.7788	0.5835	0.4250
Azimuth AOD (degree)	9.4723	6.3123	3.5078
Elevation AOD (degree)	7.4976	3.6565	2.0295
Azimuth AOA (degree)	4.0005	2.9378	1.4150
Elevation AOA (degree)	4.2699	2.1960	1.0063

B. Channel Estimation

We compare the capability of the proposed algorithm to estimate the cluster mean and spread of the multipath parameters using the root-mean-square error (RMSE) for various levels of signal-to-noise ratio (SNR), defined as SNR $= \|\mathcal{Y} - \mathcal{N}\|_F^2 / \|\mathcal{N}\|_F^2$, where $\|\cdot\|_F$ denotes the tensor Frobenius norm [34], and S and α_R are shown in Tables I–III. The results are obtained for 100 independent runs.

From Table I (impact of SNR), we observe that the estimation performance improves with SNR. The AOD has a degradation at high SNR, which we attribute to an outlier. The cluster spread estimation also improves with higher SNR. In Table II (impact of S), we note that when the S parameters increases (more diffuse scattering power), the RMSE performance of the cluster mean and cluster spread both improve. This can be ascribed to more power being available per cluster for a larger value of S. Finally, Table III (impact of α_R) reveals that when α_R increases (more smooth surface), the RMSE performance of the cluster mean improves, since the paths are more closely clustered around the mean. The cluster spread RMSE improves somewhat, though the spread itself depends on α_R.

TABLE II
RMSE OF CLUSTER MEAN (TOP) AND SPREAD (BOTTOM) - DENSE
COMPONENTS, FOR VARIOUS LEVELS OF SCATTER PARAMETER

RMSE	Scatter Parameter S		
SNR = 10 dB, $\alpha_R = 10$	0.4	0.6	0.8
Delay (meter)	0.6774	0.2033	0.1587
Azimuth AOD (degree)	2.7009	2.4131	2.1715
Elevation AOD (degree)	2.8291	3.0790	3.0189
Azimuth AOA (degree)	2.8190	1.5043	1.4027
Elevation AOA (degree)	1.9688	1.2875	1.2407

RMSE	Scatter Parameter S		
SNR = 10 dB, $\alpha_R = 10$	0.4	0.6	0.8
Delay (meter)	0.5078	0.4553	0.4250
Azimuth AOD (degree)	4.5017	4.9590	4.6179
Elevation AOD (degree)	2.2973	2.3543	2.1723
Azimuth AOA (degree)	4.1994	1.7163	1.7888
Elevation AOA (degree)	1.2629	1.0384	1.0303

TABLE III
RMSE OF CLUSTER MEAN (TOP) AND SPREAD (BOTTOM) - DENSE
COMPONENTS, FOR VARIOUS LEVELS OF ROUGHNESS PARAMETER

RMSE	Roughness α_R		
SNR = 10 dB, $S = 0.8$	0	10	20
Delay (meter)	0.4377	0.1587	0.1224
Azimuth AOD (degree)	6.4553	2.1715	1.8097
Elevation AOD (degree)	3.1283	3.0189	2.5473
Azimuth AOA (degree)	5.2559	1.4027	0.9615
Elevation AOA (degree)	1.8629	1.2407	1.1137

RMSE	Roughness α_R		
SNR = 10 dB, $S = 0.8$	0	10	20
Delay (meter)	1.0373	0.4250	0.2694
Azimuth AOD (degree)	10.8263	4.6179	3.5078
Elevation AOD (degree)	2.7932	2.1723	2.0295
Azimuth AOA (degree)	6.0143	1.7888	1.4150
Elevation AOA (degree)	1.5066	1.0303	1.0063

Fig. 4. Positioning in LOS utilizing all the resolved paths: RMSE versus SNR (top), roughness α_R (middle) and scattering parameter S (bottom).

C. Positioning and Mapping in LOS

The setup is the same as in the Fig. 3, but now it also includes the LOS path. Fig. 4 shows the positioning RMSE performance for different SNR, α_R and S, with weights $\zeta_k = 1$. We observe that thanks to the antenna gains, sub-meter positioning accuracy is achieved when the SNR > -10 dB. Lower RMSE is achieved with larger scattering parameter S. Furthermore, positioning accuracy is sensitive to α_R, with more rough surfaces leading to larger RMSE, especially at lower SNRs.

Fig. 5 shows the positioning performance of utilizing the LOS path and LOS path plus four different combinations of the diffuse paths, which is given by:

1) Mean path for each cluster (Mean)
2) Shortest delay path for each cluster (Shortest Path)
3) All paths for each cluster (All Paths)
4) First 2 paths for each cluster (First 2 Paths).

Compared with the other four algorithms, larger positioning error occurs for the Mean algorithm. That is because just compute the means is not a good approximation of the specular path. Lowest RMSE is achieved by only utilizing the LOS path. That is because when the LOS path is present, the NLOS paths mainly create disturbances, with more diffuse paths leading to larger RMSE.
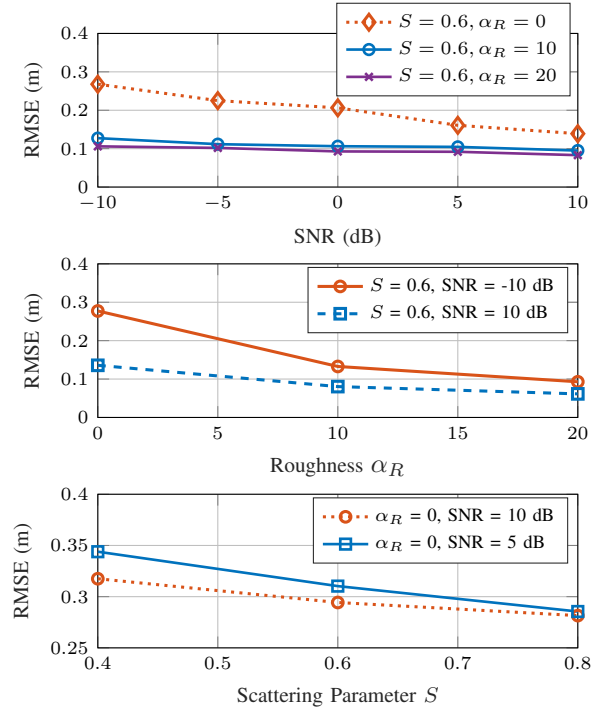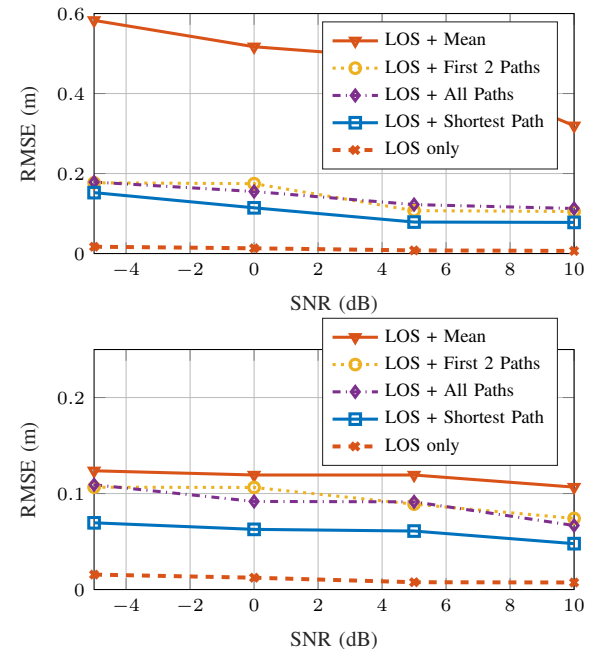

Fig. 5. Positioning in LOS utilizing all the resolved paths: RMSE versus SNR for different algorithms, $S = 0.6$, $\alpha_R = 0$ (top) and $\alpha_R = 10$ (bottom).
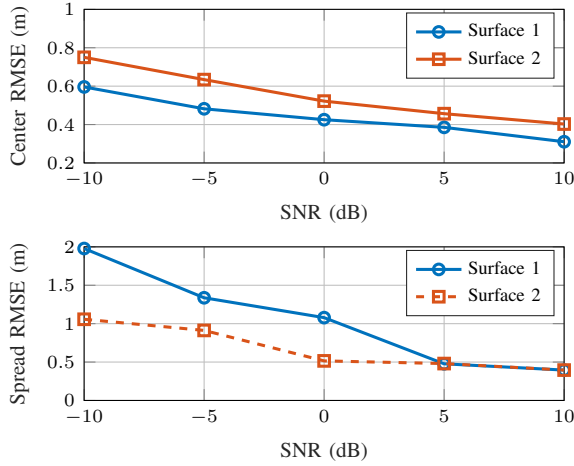
Fig. 6. Mapping in LOS utilizing all the resolved paths: RMSE of estimated center and spread of the reflective surfaces versus SNR, $\alpha_R = 10$ and $S = 0.6$.
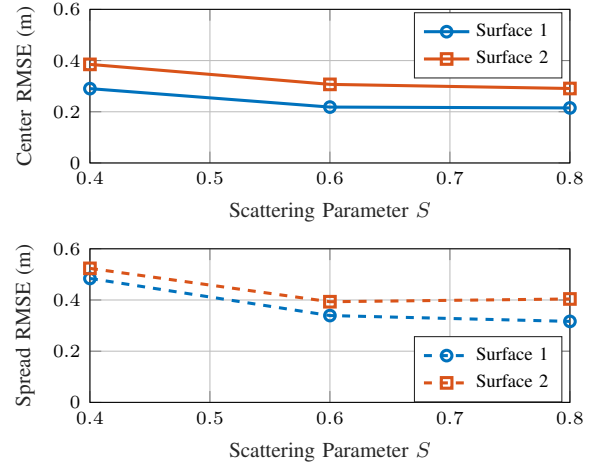

Fig. 8. Mapping in LOS utilizing all the resolved paths: RMSE of estimated center and spread of the reflective surfaces versus scattering parameter S, $\alpha_R = 10$ and SNR = 10 dB.
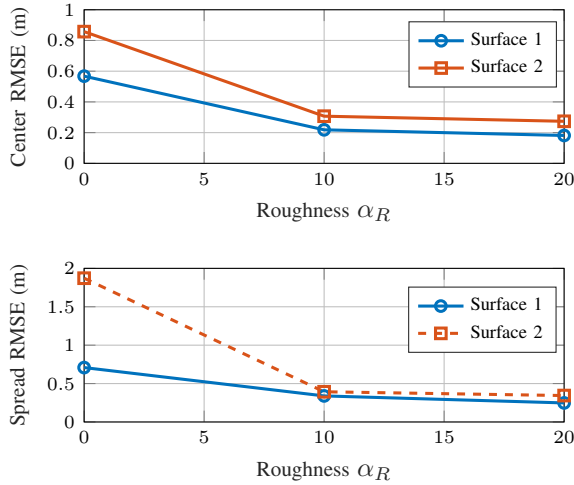

Fig. 7. Mapping in LOS utilizing all the resolved paths: RMSE of estimated center and spread of the reflective surfaces versus roughness parameter $S = 0.6$ and SNR = 10 dB.
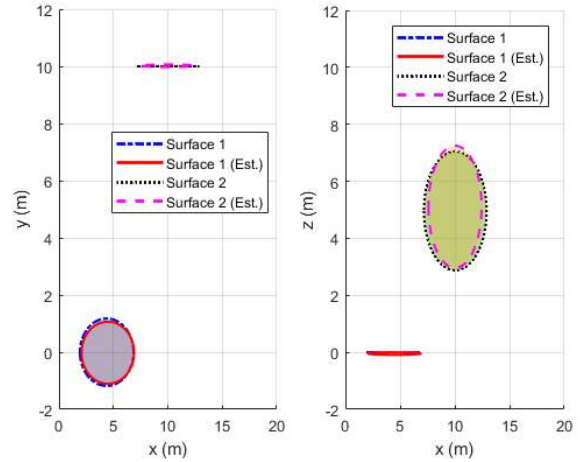

Fig. 9. Mapping in LOS utilizing all the resolved paths: Comparison of the actual and estimated reflective surfaces, projection onto the x-y plane (left) and x-z plane (right), SNR = 10 dB, $\alpha_R = 10$ and $S = 0.6$.

D. Positioning and Mapping in NLOS

We now move on to the more challenging scenario without LOS. The system setup is the one shown in Fig. 3 and all the resolved paths are utilized for positioning and mapping. Figure 10 shows the positioning RMSE performance for different SNR and α_R. Similar to LOS scenarios, high SNR is also helpful for positioning in NLOS. Another observation is that lower RMSE is achieved by increasing the roughness parameter α_R. Overall, performance is somewhat worse than in LOS.

Fig. 11 shows the positioning performance in NLOS scenarios. The diffuse paths are helpful to improve the position accuracy. Lower positioning error is achieved by utilizing more diffuse paths and best performance is achieved by using all the estimated diffuse paths. Furthermore, positioning accuracy is sensitive to α_R, with more rough surfaces leading to larger RMSE.

To assess the mapping performance, the RMSE of estimated

The mapping performance is evaluated in terms of the accuracy of the estimated center and spread of the reflective surfaces (clusters). Note that mapping is performed jointly with positioning. The center and spread are defined as the mean and standard deviation of all the estimated $\hat{p}_k$ within the same cluster. RMSE of estimated center and spread of the reflective surfaces versus SNR are shown in Fig. 6. As we expected, high SNR is helpful for center and spread estimation. Mapping performance versus scattering parameters are shown in Fig. 7–8. Similar to the positioning performance in Fig. 4, lower RMSE is achieved for larger α_R and larger S.

The actual and estimated reflective surfaces projected onto the x-y plane and x-z plane are shown in Fig. 9. There is a good match between the actual and the estimated surface, since both the SNR and α_R value are large.
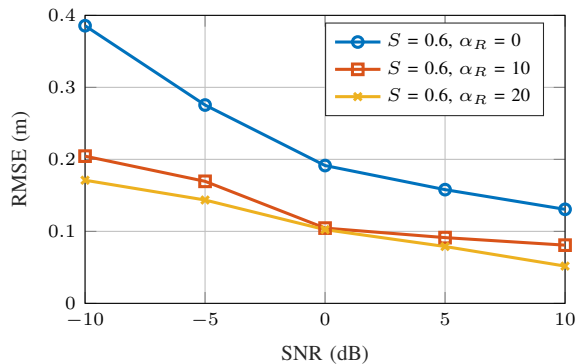
Fig. 10. Positioning in NLOS utilizing all the resolved paths: RMSE versus SNR for different values of the scattering parameters.
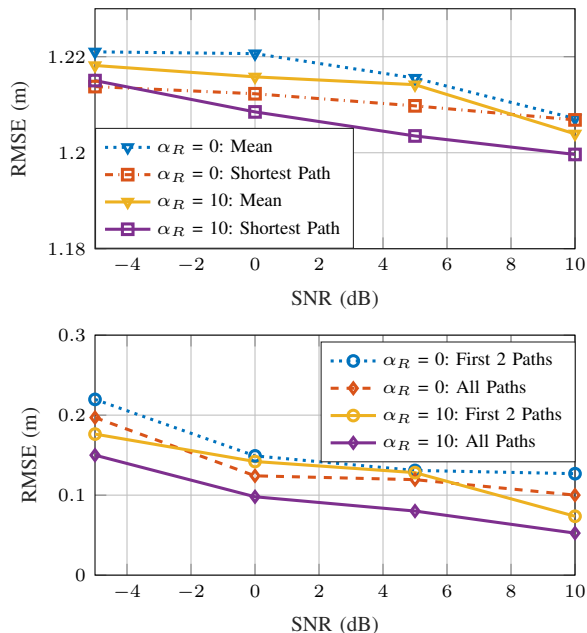

Fig. 11. Positioning in NLOS: RMSE versus SNR for different algorithms, $S = 0.6$, mean or the shortest path (top) and the first two paths per cluster or all paths (bottom).
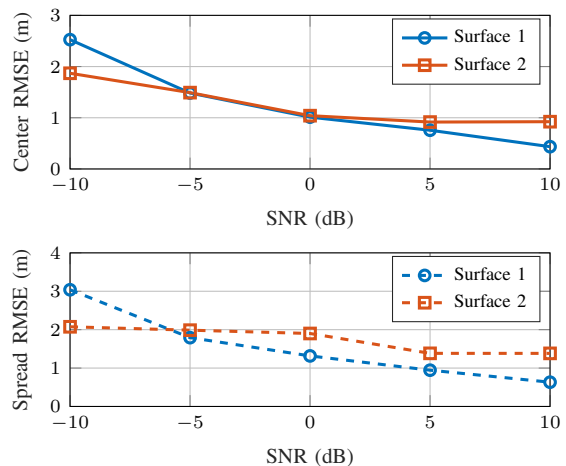

Fig. 12. Mapping in NLOS utilizing all the resolved paths: RMSE of estimated center and spread of the reflective surfaces versus SNR in NLOS, $\alpha_R = 10$ and $S = 0.6$.
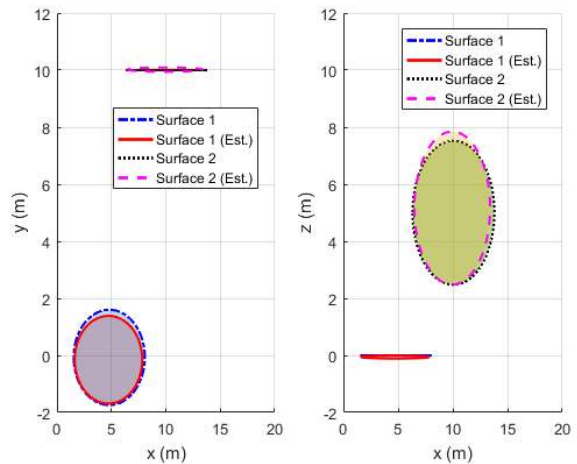

Fig. 13. Mapping in NLOS utilizing all the resolved paths: Comparison of the actual and estimated reflective surfaces in NLOS, projection onto the x-y plane (left) and x-z plane (right), SNR = -10 dB, $\alpha_R = 0$ and $S = 0.6$.

center and spread of the reflective surfaces versus SNR in NLOS are shown in Fig. 12. Note again that mapping is performed jointly with positioning, so the receiver's position is not known. From Fig. 12, we observe that there is a performance penalty compared to the LOS case, but at sufficiently high SNR, accurate center and spread estimates can be obtained.

The actual and estimated reflective surfaces projected onto the x-y plane and x-z plane in NLOS are shown in Fig. 13. The mapping error is slightly larger when compared with the LOS scenarios, because the estimated receiver position is more accurate with LOS.

VI. CONCLUSION

We have studied the problem of channel estimation of mmWave channels with diffuse scattering components, combined with positioning and mapping. We proposed a novel tensor-based method for estimation of the mmWave channel parameters in a non-parametric form. Reflective surfaces with different roughness and scattering parameters are considered. The method is able to accurately estimate the channel, center and spread of the reflective surfaces, even in the absence of a specular component. We also propose a low complexity, search-free method for localization and mapping based on these channel estimates, and demonstrate that accurate localization of a user and mapping of the environment is possible, even when the LOS path is blocked and surfaces are characterized by only diffuse scattering.

APPENDIX A
GEOMETRIC RELATIONS

The geometric relations between the location parameters are as follows, with $\boldsymbol{p}_T = [x_T, y_T, z_T]^\mathsf{T}$, $\boldsymbol{p}_R = [x_R, y_R, z_R]^\mathsf{T}$, $\boldsymbol{p}_{kl} = [x_{kl}, y_{kl}, z_{kl}]^\mathsf{T}$:

- TOA: $\tau_{kl} = \|\boldsymbol{p}_{kl} - \boldsymbol{p}_T\|/c + \|\boldsymbol{p}_{kl} - \boldsymbol{p}_R\|/c$

- AOA azimuth: $\vartheta_{kl} = \arctan 2\left(y_{kl} - y_{\mathrm{R}}, x_{kl} - x_{\mathrm{R}}\right) + \pi$.
- AOA elevation: $\varphi_{kl} = \arccos\left((z_{kl} - z_{\mathrm{R}})/\|\boldsymbol{p}_{kl} - \boldsymbol{p}_{\mathrm{R}}\|\right)$.
- AOD azimuth: $\theta_{kl} = \arctan 2\left(y_{kl} - y_{\mathrm{T}}, x_{kl} - x_{\mathrm{T}}\right)$.
- AOD elevation: $\phi_{kl}=\arccos\left((z_{kl} - z_{\mathrm{T}})/\|\boldsymbol{p}_{kl} - \boldsymbol{p}_{\mathrm{T}}\|\right)$.

Appendix B
Generation of scatter points and their complex gains

Clearly, $p_{\mathrm{DM}}(\boldsymbol{p}) = 0$ for any $\boldsymbol{p}$ not lying on a surface. To populate the k-th rough surface $\mathbb{S}_k$ with scatter points $\{\boldsymbol{p}_{kl}\} \subseteq \mathbb{S}_k, 0 < l \le L_k$, we decompose $p_{\mathrm{DM}}(\boldsymbol{p}) = \sum_k p_{\mathrm{DM},k}(\boldsymbol{p})$ where $p_{\mathrm{DM},k}(\boldsymbol{p})$ denotes the JADPS associated to k. The JADPS is calculated as function of $\boldsymbol{p}_{\mathrm{T}}$, $\boldsymbol{p}_{\mathrm{R}}$, surface location, as well as S and α_R [30].

To generate the scatter points as well as the complex gains, we consider two methods:

- *Rejection sampling:* We generate the scatter points $\boldsymbol{p}_{kl}$ such that their density on $\mathbb{S}_k$ is proportional to $p_{\mathrm{DM},k}(\boldsymbol{p})$. Then, $p_{\mathrm{DM},k}(\boldsymbol{p})$ can be approximated as $\sum_{l=1}^{L_k} |\gamma_{kl}|^2 \delta(\boldsymbol{p} - \boldsymbol{p}_{kl})$ with Dirac delta δ and $\boldsymbol{p}_{kl}$ resulting from rejection sampling [39]. The corresponding γ_{kl} is set equal magnitude $|\gamma_{kl}| = \sqrt{\frac{1}{L_k} P_{k,\mathrm{total}}}$, $P_{k,\mathrm{total}} = \int_{\mathbb{S}_k} p_{\mathrm{DM},k}(\boldsymbol{p}) \mathrm{d}x\mathrm{d}y\mathrm{d}z$ and random phase, uniform over $[0, 2\pi)$. This procedure allows to describe the JADPS with a rather small L_k.
- *Uniform sampling:* As an alternative, $\boldsymbol{p}_{kl}$ may be distributed uniformly onto $\mathbb{S}_k$. The corresponding γ_{kl} are sampled from a zero-mean Normal distribution with variance $p_{\mathrm{DM},k}(\boldsymbol{p})$, i.e., γ_{kl} has a zero-mean, complex-valued, circularly symmetric gain γ_{kl} [5] with $\mathbb{E}[|\gamma_{kl}|^2] = p_{\mathrm{DM}}(\boldsymbol{p}_{kl}) \equiv p_{\mathrm{DM}}(\theta_{kl}, \phi_{kl}, \vartheta_{kl}, \varphi_{kl}, \tau_{kl})$.

For large surfaces, the large dynamic of the JADPS results in almost zero gain of many $\boldsymbol{p}_{kl}$ in the second method, while the first method omits regions in $\mathbb{S}_k$ with small JADPS. Hence, we propose the use of the first method and have used in throughout this current work.

References

[1] H. Wymeersch, G. Seco-Granados, G. Destino, D. Dardari, and F. Tufvesson, "5G mmwave positioning for vehicular networks," *IEEE Wireless Communications*, vol. 24, no. 6, pp. 80–86, 2017.

[2] K. Witrisal, P. Meissner, E. Leitinger, Y. Shen, C. Gustafson, F. Tufvesson, K. Haneda, D. Dardari, A. F. Molisch, A. Conti, and M. Z. Win, "High-accuracy localization for assisted living: 5G systems will turn multipath channels from foe to friend," *IEEE Signal Processing Magazine*, vol. 33, no. 2, pp. 59–70, March 2016.

[3] M. R. Akdeniz, Y. Liu, M. K. Samimi, S. Sun, S. Rangan, T. S. Rappaport, and E. Erkip, "Millimeter wave channel modeling and cellular capacity evaluation," *IEEE Journal on Selected Areas in Communications*, vol. 32, no. 6, pp. 1164–1179, 2014.

[4] B. H. Fleury, "First-and second-order characterization of direction dispersion and space selectivity in the radio channel," *IEEE Transactions on Information Theory*, vol. 46, no. 6, pp. 2027–2044, 2000.

[5] O. Besson and P. Stoica, "Decoupled estimation of DOA and angular spread for a spatially distributed source," *IEEE Transactions on Signal Processing*, vol. 48, no. 7, pp. 1872–1882, 2000.

[6] T. Yucek and H. Arslan, "Time dispersion and delay spread estimation for adaptive OFDM systems," *IEEE Transactions on Vehicular Technology*, vol. 57, no. 3, pp. 1715–1722, 2008.

[7] S. Shahbazpanahi, S. Valaee, and M. H. Bastani, "Distributed source localization using ESPRIT algorithm," *IEEE Transactions on Signal Processing*, vol. 49, no. 10, pp. 2169–2178, Oct 2001.

[8] G. Li, J. Xu, Y.-N. Peng, and X.-G. Xia, "A low-complexity estimator for incoherently distributed sources with narrow or wide spread angles," *Signal Processing*, vol. 87, no. 5, pp. 1058–1065, 2007.

[9] A. Zoubir, Y. Wang, and P. ChargÉ, "Efficient subspace-based estimator for localization of multiple incoherently distributed sources," *IEEE Transactions on Signal Processing*, vol. 56, no. 2, pp. 532–542, Feb 2008.

[10] Z. Dai, B. Ba, W. Cui, and Y. Sun, "Computational efficient two-dimension DOA estimation for incoherently distributed noncircular sources with automatic pairing," *IEEE Access*, vol. 5, pp. 20 249–20 259, 2017.

[11] J. Lee, I. Song, H. Kwon, and S. R. Lee, "Low-complexity estimation of 2D DOA for coherently distributed sources," *Signal Processing*, vol. 83, no. 8, pp. 1789 – 1802, 2003.

[12] A. Zoubir and Y. Wang, "Efficient DSPE algorithm for estimating the angular parameters of coherently distributed sources," *Signal Processing*, vol. 88, no. 4, pp. 1071 – 1078, 2008.

[13] Y. Zhou, Z. Fei, S. Yang, J. Kuang, S. Chen, and L. Hanzo, "Joint angle estimation and signal reconstruction for coherently distributed sources in massive MIMO systems based on 2-D unitary ESPRIT," *IEEE Access*, vol. 5, pp. 9632–9646, 2017.

[14] H. Yan, V. Boljanovic, and D. Cabric, "Tracking sparse mmwave channel: Performance analysis under intra-cluster angular spread," in *IEEE 19th International Workshop on Signal Processing Advances in Wireless Communications*, Kalamata, Greece, June 2018, pp. 1–5.

[15] A. Shahmansoori, G. E. Garcia, G. Destino, G. Seco-Granados, and H. Wymeersch, "Position and orientation estimation through millimeter-wave MIMO in 5G systems," *IEEE Transactions on Wireless Communications*, vol. 17, no. 3, pp. 1822–1835, 2018.

[16] R. Mendrzik, F. Meyer, G. Bauch, and M. Z. Win, "Enabling situational awareness in millimeter wave massive mimo systems," *IEEE Journal of Selected Topics in Signal Processing*, vol. 13, no. 5, pp. 1196–1211, 2019.

[17] H. Wymeersch, N. Garcia, H. Kim, G. Seco-Granados, S. Kim, F. Went, and M. Fröhle, "5G mm wave downlink vehicular positioning," in *2018 IEEE Global Communications Conference (GLOBECOM)*. IEEE, 2018, pp. 206–212.

[18] A. Alkhateeb, O. El Ayach, G. Leus, and R. W. Heath, "Channel estimation and hybrid precoding for millimeter wave cellular systems," *IEEE Journal of Selected Topics in Signal Processing*, vol. 8, no. 5, pp. 831–846, 2014.

[19] Z. Zhou, J. Fang, L. Yang, H. Li, Z. Chen, and S. Li, "Channel estimation for millimeter-wave multiuser MIMO systems via parafac decomposition," *IEEE Transactions on Wireless Communications*, vol. 15, no. 11, pp. 7501–7516, 2016.

[20] Z. Zhou, J. Fang, L. Yang, H. Li, Z. Chen, and R. S. Blum, "Low-rank tensor decomposition-aided channel estimation for millimeter wave MIMO-OFDM systems," *IEEE Journal on Selected Areas in Communications*, vol. 35, no. 7, pp. 1524–1538, 2017.

[21] M. Ruble and I. Güvenç, "Multilinear singular value decomposition for millimeter wave channel parameter estimation," *IEEE Access*, pp. 1–1, 2020.

[22] M. Ester, H.-P. Kriegel, J. Sander, and X. Xu, "A density-based algorithm for discovering clusters in large spatial databases with noise," in *Proceedings of the Second International Conference on Knowledge Discovery and Data Mining*, 1996, pp. 226–231.

[23] F. Wen and H. Wymeersch, "5G synchronization, positioning, and mapping from diffuse multipath," *IEEE Wireless Communications Letters*, pp. 1–1, 2020.

[24] M. Haardt, F. Roemer, and G. Del Galdo, "Higher-order SVD-based subspace estimation to improve the parameter estimation accuracy in multidimensional harmonic retrieval problems," *IEEE Transactions on Signal Processing*, vol. 56, no. 7, pp. 3198–3213, 2008.

[25] L. De Lathauwer, B. De Moor, and J. Vandewalle, "A multilinear singular value decomposition," *SIAM Journal on Matrix Analysis and Applications*, vol. 21, no. 4, pp. 1253–1278, 2000.

[26] F. Roemer and M. Haardt, "Tensor-structure structured least squares (TS-SLS) to improve the performance of multi-dimensional Esprit-type algorithms," in *IEEE International Conference on Acoustics, Speech and Signal Processing*, vol. 2, April 2007, pp. II–893–II–896.

[27] J. P. C. L. da Costa, F. Roemer, M. Haardt, and R. T. de Sousa, "Multi-dimensional model order selection," *EURASIP Journal on Advances in Signal Processing*, vol. 2011, no. 1, p. 26, Jul 2011.

[28] K. Liu, J. P. C. da Costa, H. C. So, L. Huang, and J. Ye, "Detection of number of components in candecomp/parafac models via minimum description length," *Digital Signal Processing*, vol. 51, pp. 110 – 123, 2016.

[29] T. Yokota, N. Lee, and A. Cichocki, "Robust multilinear tensor rank estimation using higher order singular value decomposition and information criteria," *IEEE Transactions on Signal Processing*, vol. 65, no. 5, pp. 1196–1206, March 2017.

[30] J. Kulmer, F. Wen, N. Garcia, H. Wymeersch, and K. Witrisal, "Impact of rough surface scattering on stochastic multipath component models," in *2018 IEEE 29th Annual International Symposium on Personal, Indoor and Mobile Radio Communications (PIMRC)*. IEEE, 2018, pp. 1410–1416.

[31] V. Degli-Esposti, F. Fuschini, E. M. Vitucci, and G. Falciasecca, "Measurement and modelling of scattering from buildings," *IEEE Transactions on Antennas and Propagation*, vol. 55, no. 1, pp. 143–153, 2007.

[32] J. Järveläinen and K. Haneda, "Sixty gigahertz indoor radio wave propagation prediction method based on full scattering model," *Radio Science*, vol. 49, no. 4, pp. 293–305, 2014.

[33] Z. Sha, Z. Wang, and S. Chen, "Harmonic retrieval based baseband channel estimation for millimeter wave OFDM systems," *IEEE Transactions on Vehicular Technology*, vol. 68, no. 3, pp. 2668–2681, March 2019.

[34] T. G. Kolda and B. W. Bader, "Tensor decompositions and applications," *SIAM Review*, vol. 51, no. 3, pp. 455–500, Aug. 2009.

[35] F. Roemer, M. Haardt, and G. D. Galdo, "Analytical performance assessment of multi-dimensional matrix- and tensor-based ESPRIT-type algorithms," *IEEE Transactions on Signal Processing*, vol. 62, no. 10, pp. 2611–2625, May 2014.

[36] S. Sahnoun, K. Usevich, and P. Comon, "Multidimensional ESPRIT for damped and undamped signals: Algorithm, computations, and perturbation analysis," *IEEE Transactions on Signal Processing*, vol. 65, no. 22, pp. 5897–5910, Nov. 2017.

[37] F. Wen, N. Garcia, J. Kulmer, K. Witrisal, and H. Wymeersch, "Tensor decomposition based beamspace ESPRIT for millimeter wave MIMO channel estimation," in *2018 IEEE Global Communications Conference*, Dec 2018, pp. 1–7.

[38] A. K. Jain, "Data clustering: 50 years beyond K-means," *Pattern Recognition Letters*, vol. 31, no. 8, pp. 651 – 666, 2010, Award winning papers from the 19th International Conference on Pattern Recognition (ICPR).

[39] C. M. Bishop, *Pattern Recognition and Machine Learning*. New York, USA: Springer, 2006.

[40] R. He, B. Ai, A. F. Molisch, G. L. Stuber, Q. Li, Z. Zhong, and J. Yu, "Clustering enabled wireless channel modeling using big data algorithms," *IEEE Communications Magazine*, vol. 56, no. 5, pp. 177–183, 2018.

[41] Q. Wang, B. Ai, R. He, K. Guan, Y. Li, Z. Zhong, and G. Shi, "A framework of automatic clustering and tracking for time-variant multipath components," *IEEE Communications Letters*, vol. 21, no. 4, pp. 953–956, 2017.

[42] H. Wymeersch, "A simple method for 5G positioning and synchronization without line-of-sight," 2018, arXiv:1812.05417.

[43] H. Kim, K. Granström, L. Gao, G. Battistelli, S. Kim, and H. Wymeersch, "5G mmwave cooperative positioning and mapping using multimodel PHD filter and map fusion," *IEEE Transactions on Wireless Communications*, pp. 1–1, 2020.

[44] A. Liu, L. Lian, V. Lau, G. Liu, and M. Zhao, "Cloud-assisted cooperative localization for vehicle platoons: A turbo approach," *IEEE Transactions on Signal Processing*, vol. 68, pp. 605–620, 2020.

[45] A. Phan, P. Tichavský, and A. Cichocki, "CANDECOMP/PARAFAC decomposition of high-order tensors through tensor reshaping," *IEEE Transactions on Signal Processing*, vol. 61, no. 19, pp. 4847–4860, 2013.

[46] N. Vervliet, O. Debals, L. Sorber, M. Van Barel, and L. De Lathauwer. (2016, Mar.) Tensorlab 3.0. [Online]. Available: https://www.tensorlab.net

[47] F. Wen, H. C. So, and H. Wymeersch, "Tensor decomposition-based beamspace ESPRIT algorithm for multidimensional harmonic retrieval," in *IEEE International Conference on Acoustics, Speech and Signal Processing (ICASSP)*, 2020, pp. 4572–4576.

Fuxi Wen (M'09–SM'19) received the Ph.D. degree in Electrical and Electronic Engineering from Nanyang Technological University, Singapore, in 2013. He held research positions in Singapore and the United Kingdom, from 2013 to 2017. He was a Researcher and Marie Skłodowska-Curie Fellow with the Department of Electrical Engineering, Chalmers University of Technology, Sweden, from 2017 to 2020. He has served as the Secretary of the IEEE Signal Processing Society, Sweden Chapter, since 2018. He joined Tsinghua University as a Research Associate Professor in 2020. His research interests include tensor-based signal processing, situational awareness-enabled wireless communications, and their applications in mmWave and vehicular communications.

Josef Kulmer (S'15) received the M.Sc. degree in electrical engineering and audio engineering from the University of Music and Performing Arts, Graz, in 2014, and the Ph.D. degree in electrical engineering from Graz University of Technology, in 2019.,His current research interests include linear algebra, exploration of space, and microwaves.

Klaus Witrisal (S'98–M'03) received the Ph.D. degree (cum laude) from the Delft University of Technology, Delft, The Netherlands, in 2002, and the Habilitation degree from the Graz University of Technology, in 2009. He is currently an Associate Professor with the Signal Processing and Speech Communication Laboratory (SPSC), Graz University of Technology, and the Head of the Christian Doppler Laboratory for Location-Aware Electronic Systems. His research interests are in signal processing for wireless communications, propagation channel modeling, and positioning. He has served as an Associate Editor of the IEEE Communications Letters, the Co-Chair of the TWG Indoor of the COST Action IC1004, the Co-Chair of the EWG Localization and Tracking of the COST Action CA15104, the leading Chair of the IEEE Workshop on Advances in Network Localization and Navigation (ANLN), and the TPC (Co)-Chair of the Workshop on Positioning, Navigation, and Communication (WPNC).

Henk Wymeersch (S'01, M'05, SM'19) obtained the Ph.D. degree in Electrical Engineering/Applied Sciences in 2005 from Ghent University, Belgium. He is currently a Professor of Communication Systems with the Department of Electrical Engineering at Chalmers University of Technology, Sweden. He is also a Distinguished Research Associate with Eindhoven University of Technology. Prior to joining Chalmers, he was a postdoctoral researcher from 2005 until 2009 with the Laboratory for Information and Decision Systems at the Massachusetts Institute of Technology. Prof. Wymeersch served as Associate Editor for IEEE Communication Letters (2009-2013), IEEE Transactions on Wireless Communications (since 2013), and IEEE Transactions on Communications (2016-2018). During 2019-2021, he is a IEEE Distinguished Lecturer with the Vehicular Technology Society. His current research interests include the convergence of communication and sensing, in a 5G and Beyond 5G context.